

Article

Continuous Flow Photocatalytic Degradation of Phenol Using Palladium@Mesoporous TiO₂ Core@Shell Nanoparticles

Moses T. Yilleng^{1,2}, Nancy Artioli^{1,3}, David Rooney¹ and Haresh Manyar^{1,*}

¹ School of Chemistry and Chemical Engineering, Queen's University Belfast, David-Keir Building, Stranmillis Road, Belfast BT9 5AG, UK; yilleng@yahoo.com (M.T.Y.); nancy.artioli@unibs.it (N.A.); d.rooney@qub.ac.uk (D.R.)

² Department of Chemistry, Kaduna State University, Tafawa Balewa Way, Kaduna 800001, Kaduna State, Nigeria

³ Department of Civil, Environmental, Architectural Engineering and Mathematics, University of Brescia, Via Branze, 43, 25123 Brescia, Italy

* Correspondence: h.manyar@qub.ac.uk

Abstract: Palladium@mesoporous titania core@shell nanoparticles with uniform and narrow particle size distribution were synthesised using a four component “water in oil” microemulsion system. The prepared materials were well characterised using N₂ adsorption–desorption measurements, temperature program oxidation, X-ray diffraction, ICP-OES, DRS UV-Vis, PL, TGA and transmission electron microscopy techniques. The core@shell nanoparticles showed very good absorption in both the UV and visible regions and a low bandgap, indicating that the prepared materials are visible-light-active, unlike the pristine TiO₂ P25. The activity of the prepared materials was evaluated in the photodegradation of phenol using both UV and visible light, in batch and continuous flow trickle-bed and Taylor flow photoreactors. The prepared 2%Pd@mTiO₂ core@shell nanoparticles showed better photocatalytic performance for phenol degradation in visible light in comparison to pristine TiO₂ P25 and conventional 0.5%Pd/TiO₂ P25 catalysts. The TiO₂ P25 and conventional 0.5%Pd/TiO₂ P25 catalysts showed gradual catalyst deactivation due to photocorrosion, the deposition of intermediates and Pd metal leaching. In comparison, the 2%Pd@mTiO₂ catalyst showed higher catalyst stability and reusability. The 2%Pd@mTiO₂ catalysts showed very high and stable phenol degradation (97% conversion) in continuous flow over 52 h. The results showed the feasibility of utilising the developed continuous Taylor flow photoreactor for phenol degradation or as a wastewater treatment plant.

Keywords: visible light photocatalyst; Pd@TiO₂ core@shell nanoparticles; continuous flow reactor; Taylor flow; photocatalytic degradation; phenol; organic wastes



check for updates

Citation: Yilleng, M.T.; Artioli, N.; Rooney, D.; Manyar, H. Continuous Flow Photocatalytic Degradation of Phenol Using Palladium@Mesoporous TiO₂ Core@Shell Nanoparticles.

Water **2023**, *15*, 2975. <https://doi.org/10.3390/w15162975>

Academic Editor: Daniel Mamais

Received: 25 July 2023

Revised: 11 August 2023

Accepted: 17 August 2023

Published: 18 August 2023



Copyright: © 2023 by the authors. Licensee MDPI, Basel, Switzerland. This article is an open access article distributed under the terms and conditions of the Creative Commons Attribution (CC BY) license (<https://creativecommons.org/licenses/by/4.0/>).

1. Introduction

Phenols constitute one of the basic building blocks in the pharmaceutical, agrochemical and petrochemical industries, which makes it an abundant pollutant present in wastewater. The current traditional wastewater treatment processes are less effective in terms of cost and efficiency, owing to the presence of recalcitrant chemicals that have phytotoxic effects on the microorganisms responsible for the biodegradation of the organic pollutants in wastewater [1]. Hence, several studies have been performed using modified titanium dioxides as photocatalysts for the photodegradation of phenols in wastewater using UV light [2–5]. Most photocatalysts absorb UV light, which is only a small fraction of solar energy (about 3–4%). Recently, many groups have focused on the modification of TiO₂ to achieve absorption and photocatalytic activity under UV/visible light illumination. For example, the modification of TiO₂ via doping with carbon such as graphene oxide (GO) and reduced graphene oxide has been carried out [6]. In TiO₂ photocatalysts, doping with metal ions (Fe, Ag, Ni) and nitrogen has been shown to extend the light absorption in the visible region, and photocatalysts can react upon illumination with UV/visible light irradiation for the inhibition of the proliferation of *Pseudomonas aeruginosa* [7]. The single

doping and co-doping of TiO₂ with N and Ag were shown to be effective for reducing the band gap and extending the light absorption towards the visible region by surface plasmon resonance as well as decreasing the recombination rate of electron and hole pairs of TiO₂ [8]. In the recent literature, TiO₂ nanoparticles prepared using *Pulicaria undulata* extract have shown extended light absorption in the UV-visible region and improved performance in the degradation of methylene blue and methyl orange [9]. In another recent study, zinc-oxide-based ternary ZnO/Eu₂O₃/NiO nanocomposite material was shown to exhibit excellent performance in the degradation of methylene blue dye using solar irradiation [10]. The use of TiO₂ is problematic from a health point of view, and the use of photocatalysts in powder form also poses problems with regard to recovery and reuse. Hence, low-cost industrial applications are still limited, with good photocatalytic process efficiency. There are two main design criteria to improve the overall process efficiency of wastewater treatment: the first involves the catalyst design, i.e., the fabrication of a novel photocatalyst with high activity and visible light response, and the second is reactor design, i.e., the use of process intensification, which links a novel process and an efficient photoreactor [11]. Several groups have attempted to intensify the heterogeneous photocatalytic processes; however, although a variety of photocatalytic reactors have been developed and used in lab-based or pilot plant studies, the progress in the field has been relatively slow. The reactors that have been used include the annular photoreactor [12,13] the packed bed photoreactor [14], the photocatalytic Taylor vortex reactor [15], the TiO₂ fluidized-bed reactor [16], the TiO₂-coated fibreoptic cable reactor [17,18] and the swirl-flow reactor [19]. Therefore, there is still an urgent need for the improvement of the current photocatalytic photoreactors, for facile and scalable wastewater treatment technologies.

The structure and the morphology of the nanomaterials are also important catalyst design criteria to enhance photocatalytic activity and catalyst stability [20–22]. Du et al. showed the yolk–shell-structured Fe₃O₄@TiO₂ photocatalyst, which contains an Fe₃O₄ core encapsulated with a TiO₂ shell, for the highly efficient removal of tetracycline [23]. Min et al. demonstrated the fabrication of silver@mesoporous anatase TiO₂ core@shell nanoparticles and their application in photocatalysis and SERS sensing [24]. More recently, Bayles et al. used Al@TiO₂ core@shell nanoparticles as active photocatalysts for the H₂ dissociation reaction, and hot-hole-mediated methanol dehydration reaction [25]. However, there are only a few reports on the facile synthesis of core@shell nanoparticles and their application in photocatalysis, requiring the rapid development of fabrication methodologies as well as the evaluation of the photocatalytic activity of the core@shell type of nanomaterials with tuneable particle size and shell thickness.

As a continuation of our interest in the development of advanced oxidation processes [26–33] and catalysts for the abatement of hazardous environmental pollutants [34–43], in this study, we have attempted to address the concerns of the leaching of Pd used to modify TiO₂, and to improve the photoresponse of the catalyst used in our previous study [31], by using the facile microemulsion method to synthesize the Pd@mTiO₂ core@shell nanoparticles as photocatalysts, and modifying the design of the photoreactor for the degradation of phenol in water. We also compare the performance of batch and continuous flow reactors using the conventional trickle-bed and Taylor flow systems, along with different oxidants for phenol degradation.

2. Materials and Methods

2.1. Materials

All reagents used were of analytical grade. Palladium chloride, cetyltrimethylammonium bromide, 1-butanol, sodium borohydride, polyvinyl alcohol (mol. wt. = 10,000; 80% hydrolysed), methanol and n-hexane (HPLC grade) were purchased from Sigma Aldrich UK. The TiO₂ P25 photocatalyst was procured from Degussa (Evonik, Essen, Germany). O₂ gas (purity 99.5%) was purchased from BOC, UK.

2.2. Synthesis of 2%Pd@TiO₂ Nanoparticles

2.2.1. Microemulsion Preparation

Microemulsion was prepared using a modified method, as reported in our previous work [44]. The four-component “water in oil” microemulsion was formed of a cationic surfactant cetyltrimethylammonium bromide, CTAB), a cosurfactant (1-butanol), n-hexane and water. The microemulsion had [CTAB] = 0.1 M and a molar ratio between water and surfactant (W_o). In a typical microemulsion preparation, the desired amounts of alcohol, surfactant, n-hexane and water were added to a volumetric flask; for instance, 0.62 mL of deionised water was added to hexane, 108.8 mL, and stirred at 500 rpm using a magnetic stirrer bar, followed by the addition of the surfactant CTAB, 5.821 g. The required amount of cosurfactant 1-butanol, 43.92 mL, was added slowly under continued stirring. The obtained microemulsion was allowed to stand for equilibrium for 3 to 24 h. The flask was kept closed to avoid any loss of solvent by evaporation, as solvent loss could destabilise the microemulsion.

2.2.2. Preparation of 2%Pd@mTiO₂ Core@shell Nanoparticles

In a typical preparation, 2%Pd@mTiO₂ core@shell nanoparticles were synthesised using the reduction technique with NaBH₄ as the reducing agent. The microemulsion prepared as above was split into two round bottom flasks, A and B, with 60 mL each. In solution A, 1.56 mL of PdCl₂ (1 g in 100 mL deionized water) precursor was added, and in solution B, 1.56 mL of NaBH₄ (0.4677 g to 5 mL deionized water) reducing solution was added. Solution A turned light reddish in colour and solution B remained colourless. Both solution A and solution B, were mixed for 30 min, before being combined. After mixing solutions A and B, the mixture was stirred further for 30 min, and the colour of the solution turned black, indicating the formation of Pd nanoparticles upon reduction with NaBH₄. For preparation of the TiO₂ shell, 2 mL of titanium-n-butoxide, as a titanium precursor, was added slowly, and the mixture was stirred for 4 h. For recovering the 2%Pd@mTiO₂ core@shell nanoparticles, 60 mL of methanol was added to break the microemulsion, followed by centrifuging the solution at 600 rpm for 5 min. The as-prepared core@shell nanoparticles were washed with methanol and deionised water twice, followed by overnight drying at 120 °C, and subsequent calcination in air for 4 h at 300 °C.

2.2.3. Preparation of 0.5%Pd/TiO₂ P25 Catalyst

The 0.5wt%Pd supported on TiO₂ P25 conventional photocatalyst was prepared using a modified sol immobilization method [3]. To the aqueous PdCl₂ precursor solution, 1 wt% PVA was added as the stabilizing ligand (PVA/Pd, w/w ratio = 1.2), followed by the addition of freshly prepared 0.1 M NaBH₄ solution (NaBH₄/Pd, mol/mol ratio = 5) to form a brown sol. After 30 min, TiO₂ P25 was added, which was acidified to pH 1–2 using sulphuric acid, under continued stirring for 2 h. The photocatalyst was collected by filtration, and washed with deionized water, followed by drying at 120 °C overnight and subsequent calcination for 4 h in air at 300 °C.

2.3. Characterisation of 2%Pd@TiO₂ Nanoparticles

The optical characterisation of the photocatalysts was performed using a UV–vis spectrophotometer (Perkin-Elmer Lambda 6505) with a scanning speed of 300 nm/min, in the wavelength range from 250 to 800 nm. To determine the band gap of photocatalyst samples, the Tauc plot method was used for the analysis of the diffuse reflectance spectra. The Kubelka–Munk function, $[F(R)hv]^{1/2}$, was plotted as a function of photon energy ($h\nu$), and the optical edge or onset band gap energy (E_g) was calculated by linearly extrapolating the spectra from the high slope region. Photoluminescence (PL) measurements were performed using a Horiba Jobin Yvon-Fluoromax4. The excitation wavelength used was $\lambda = 385$ nm, and the emission spectra were collected in the 400–500 nm range. Structural characterization was performed by measuring X-ray diffraction patterns with Cu K α radiation (1.5405 Å), using a PANalytical X'PERT PRO diffractometer equipped with

reflection geometry, a curved graphite crystal monochromator, a NaI scintillation counter, and a nickel filter. The diffracted intensities were collected between 5 and 80° (2 θ) by scanning at 0.017° (2 θ) steps, with a counting time of 0.5 s per step. The inductively coupled plasma optical emission spectroscopy (ICP-OES) metal analysis method using a Perkin-Elmer P-1000 Spectrometer was used to evaluate the Pd metal content for the fresh and used catalysts. The BET specific surface area, BJH total pore volume and average pore diameter were measured using N₂ sorption isotherms with Micromeritics ASAP 2020. The surface properties were studied using the FEI Tecnai™ transmission electron microscope. Thermal characterization was performed with the TG-DTA Mettler Toledo instrument using a heating rate of 200 °C/min in nitrogen atmosphere. The metal dispersion was determined using the temperature-programmed reduction (TPR) by CO chemisorption using Micromeritics Autochem 2910. The carbon content of the catalyst was determined using the temperature-programmed oxidation.

2.4. Evaluation of Photocatalytic Activity

The photocatalytic activity for phenol degradation was measured using both batch and continuous flow processes. For the batch process, a sealed Pyrex reactor with a diameter of 42.7 mm and height of 210 mm was used. In the batch reactor, 0.3 g of photocatalyst was added to 100 mL of 94.11 mg/L phenol in the deionized water solution. The pH of the aqueous phenol solution was monitored during the reaction. First, the suspension was stirred in the dark, at ambient temperature, at 650 rpm for 2 h. An aliquot was taken to analyse the phenol concentration at equilibrium. The phenol and catalyst mixture was exposed to UV or visible light using a Rayonet RMR-600 reactor. The RMR-600 consists of a 279.4 × 266.7 mm chamber manufactured from Alzak aluminium. The reactor has six 8 watt UV lamps (wavelength 350 nm), with an arc length of 76.2 mm (48 lamp watts total), and for the visible light, a fluorescence lamp with a wavelength of 555 nm was used with the power density of the incident monochromatic light being 46.120 W/m². An oxygen balloon was connected to the reactor to ensure good O₂ saturation in the solution. At periodic intervals, samples were taken for HPLC. HPLC analysis was conducted using an Agilent 1100 system equipped with an Eclipse XDB-C18 reverse-phase column (3.5 μ m, 4.6 × 150 mm) and Diode Array Detector (DAD) at a wavelength of 254 nm using 50% methanol/water as the mobile phase. An example of the HPLC chromatogram is shown in the supplementary information (Figure S1).

For the continuous flow process, the photocatalytic activity of the prepared catalysts was studied using a tubular trickle-bed reactor. A typical photoreactor set up is shown in Figure 1, operating under the Taylor flow regime. The photoreactor consists of a quartz glass tube with an external diameter of 6 mm and internal diameter of 4 mm. The reaction feed was pumped through the reactor at a 3 mL min⁻¹ flow rate. A second peristaltic pump connected to the phenol feed reservoir pumped fresh solution into the reservoir at a flow rate of 0.083 mL min⁻¹. Using this approach, the photoreactor operated continuously in recycle mode, i.e., recirculation of the feed to the photoreactor with continuous making up of fresh reagent. In each experiment, 300 mL of feed containing 94.1 mg/L (1 mMol) of phenol in water was treated over a period of 52 h. A total of 1.0 g of 0.5%Pd/TiO₂ P25 was pelletized and sieved to the 450–600 μ m particle size range. At periodic intervals, aliquots were taken for HPLC analysis.

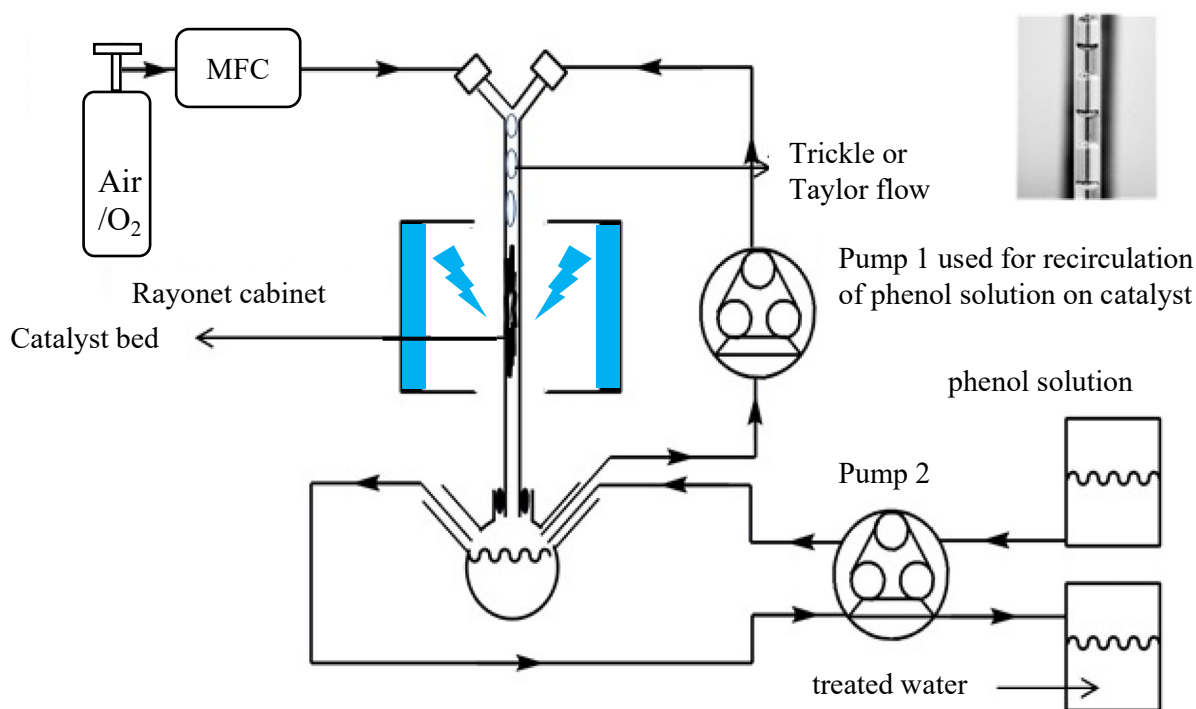


Figure 1. Schematic representation of the continuous flow photo reactor.

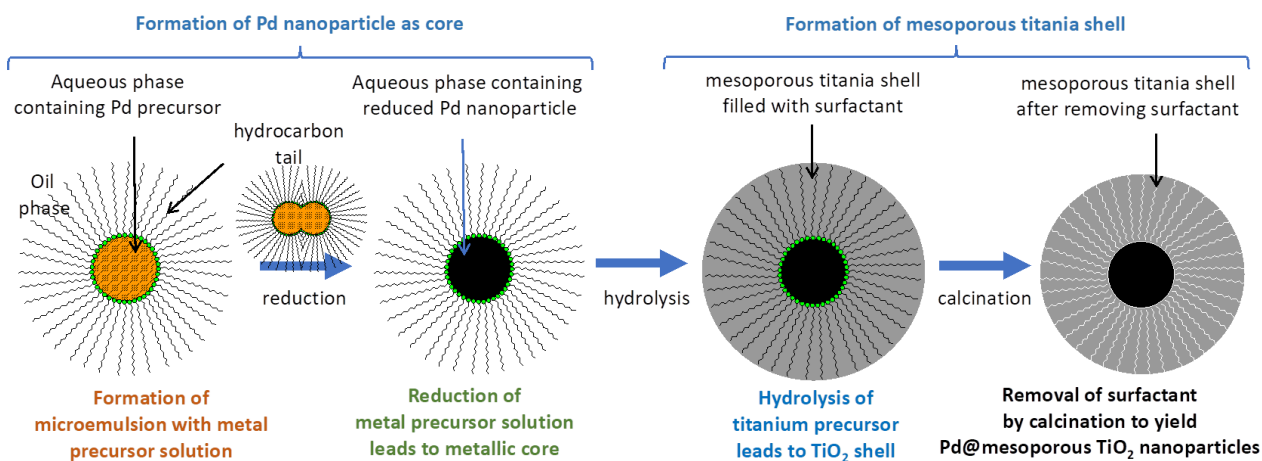
3. Results and Discussion

3.1. Catalyst Characterisation

The 2%Pd@mTiO₂ nanoparticles consist of a Pd nanoparticle as a core and a mesoporous TiO₂ shell, and the details of the fabrication process are shown in Scheme 1. In the microemulsion method, nanosized water droplets were dispersed in the continuous oil phase (hexane) and stabilized by surfactant CTAB molecules at the water/oil interface. After mixing the two microemulsions, A containing Pd precursor and B containing NaBH₄ solution, the water droplets collided with each other, exchanging the reactants, resulting in the reduction of PdCl₂ to Pd, followed by the nucleation and growth of Pd nanocrystals. CTAB molecules adsorbed onto the nanocrystals' surface to prevent them from aggregating. The formation of Pd nanoparticles is subsequently followed by the hydrolysis of titanium precursor to form mesoporous titania, which upon calcination results in mesoporous core@shell 2%Pd@mTiO₂ nanoparticles. In photocatalysis, using TiO₂, the degree of crystallinity, phase structure, and crystallite size play a significant role, with several studies showing the higher photocatalytic activity of the anatase phase of TiO₂ than the brookite or rutile phase [45]. The XRD patterns of the as-synthesised 2%Pd@mTiO₂ nanoparticles and the blank mTiO₂ shell without Pd nanoparticles are shown in Figure 2a. TiO₂ appeared to be amorphous in nature, as the peaks at 2θ values 38.6, 44.7, 65.1 and 78.5° corresponded to palladium 111, 200, 220 and 311, respectively, when compared with PDF# 84-0300. The pure amorphous titanium dioxide without palladium nanoparticles did not show any peaks on the XRD.

The DRS UV-Vis spectra of pristine TiO₂ P25, 0.5%Pd/TiO₂ P25, and 2%Pd@mTiO₂ core@shell nanoparticles are shown in Figure 2b. Both pristine TiO₂ P25, and 0.5%Pd/TiO₂ P25 showed characteristic absorption bands in the UV region at 325 nm, with no absorption in the visible region. However, the 2%Pd@mTiO₂ core@shell nanoparticles showed much broader absorption in both the UV and visible regions, indicating that 2%Pd@mTiO₂ materials are visible-light-active unlike the pristine TiO₂ P25. The absorption of the catalyst in the visible region confirms the report by Ohde et al. that the Pd nanoparticles absorb in the UV-visible region [46]. As shown in Figure 3, the modified Kubeka–Munk relation and a Tauc plot (plot of $[F(R)hv]^{1/2}$ versus photon energy, hv) were used to assess the band

gap of pristine TiO₂ P25, 0.5%Pd/TiO₂, and 2%Pd@mTiO₂ photocatalysts. Optical band gap energies were measured for O²⁻ → Ti⁴⁺ transitions in titanium dioxide and were 3.19, 3.06, and 1.67 eV for pristine TiO₂, 0.5%Pd/TiO₂, and 2%Pd@mTiO₂, respectively. For the effective absorbance of photons from visible light, the band gap should be about 1.7 eV. The observed low band gap of 1.67 eV of the 2%Pd@mTiO₂ indicates that it is an efficient visible-light-harvesting photocatalyst.



Scheme 1. Schematic representation of synthesis of 2%Pd@mTiO₂ core@shell nanoparticles.

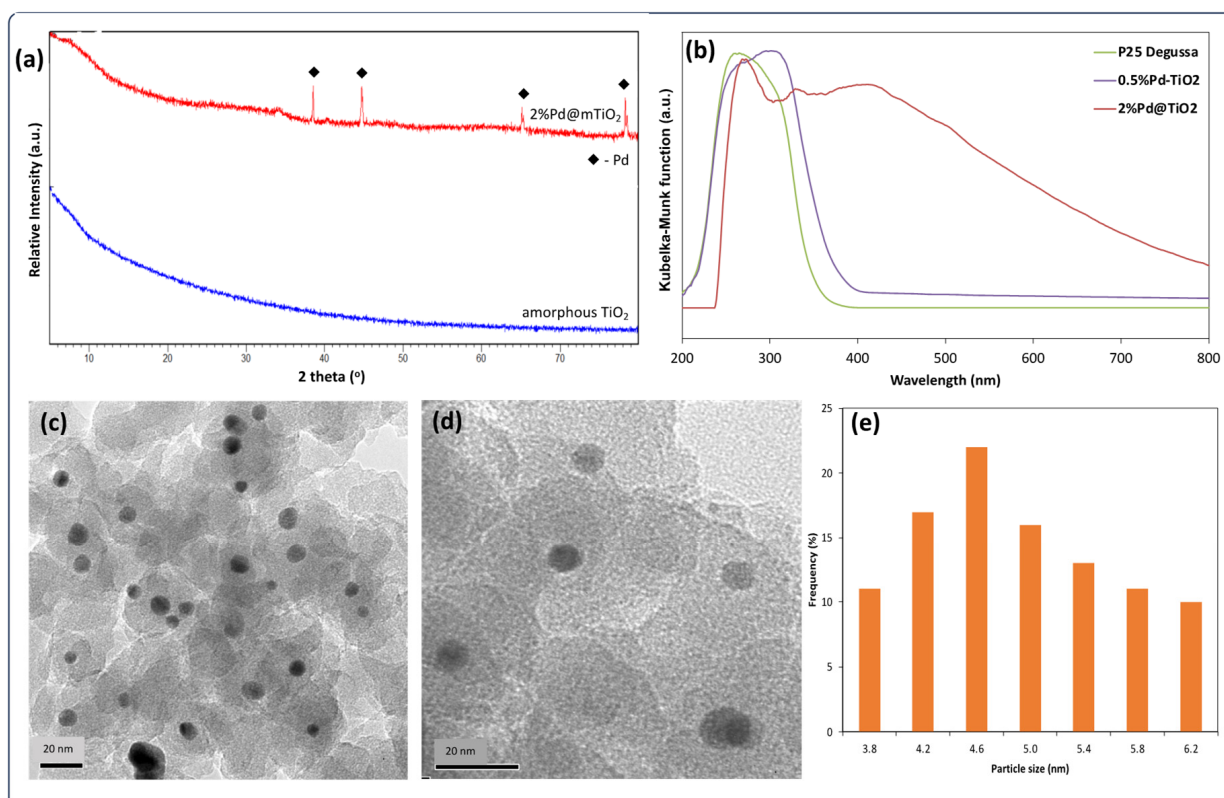


Figure 2. (a) The XRD pattern of the 2%Pd@mTiO₂ showing the presence of palladium peaks and the amorphous TiO₂. (b) The diffuse reflectance UV-Vis spectra of the 2%Pd@mTiO₂, 0.5%Pd/TiO₂ P25 and TiO₂ P25. (c,d) TEM images of 2%Pd@mTiO₂ core@shell nanoparticles, and (e) histogram showing the particle size distribution of Pd nanoparticles.

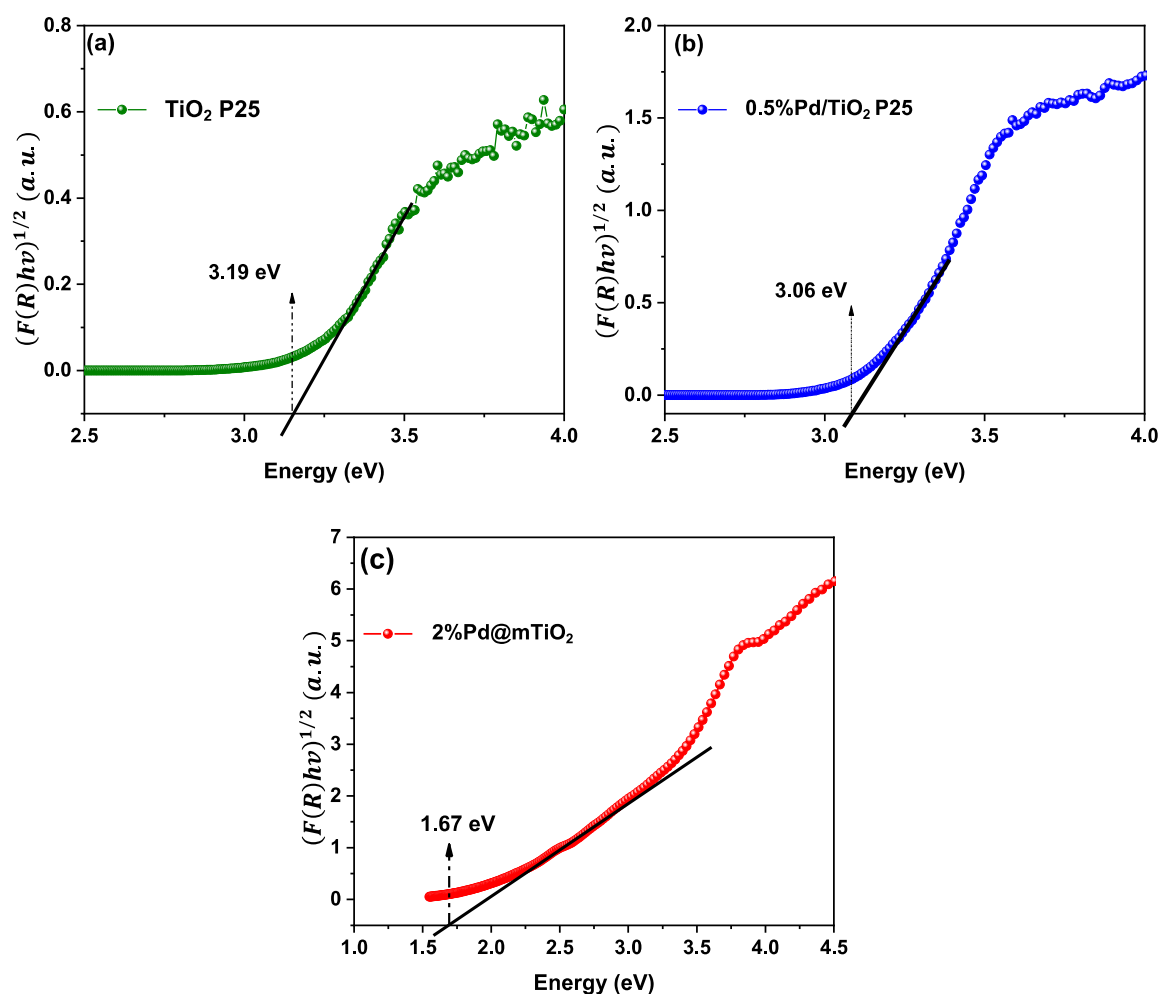


Figure 3. The Tauc plot of (a) pristine TiO₂ P25, (b) 0.5%Pd/TiO₂ and (c) 2%Pd@mTiO₂ core@shell nanoparticles.

The photoluminescence spectra of the TiO₂ P25, 0.5%Pd/TiO₂ P25 and 2%Pd@mTiO₂ core@shell materials are shown in Figure 4. All three materials showed comparable peak positions with variation in intensities. In the case of 2%Pd@mTiO₂ core@shell nanoparticles, the intensity of the peak at 478 nm reduced significantly, and it showed the lowest PL intensity among all three materials, thus indicating the relatively lower recombination rate of electron and hole pairs under the same experimental conditions. The PL intensity of 0.5%Pd/TiO₂ P25 was lower as compared to the TiO₂ P25.

The TEM images of 2%Pd@mTiO₂ nanoparticles (Figure 2c,d) showed that the Pd nanoparticles were uniform and spherical in shape with a narrow particle size distribution between 4 and 6 nm, as shown in Figure 2e. The TEM image of Pd@mTiO₂ showed a distinct contrast between the lighter outer shell and the dark inner core, confirming the successful encapsulation of the TiO₂ shells over the Pd nanoparticles.

The BET surface area and pore volumes of the catalysts were obtained using N₂ sorption analysis. The specific surface areas of pristine TiO₂ P25, and 0.5%Pd/TiO₂ P25 were measured to be 55 m²/g and 47.05 m²/g, respectively, with corresponding pore volumes of 0.19 cm³/g and 0.13 cm³/g. The reduction in surface area and pore volume is expected due to the deposition of Pd nanoparticles on the surface. The 2%Pd@mTiO₂ materials showed a significantly higher specific surface area, 190 m²/g, with a pore volume of 0.19 cm³/g. The CO pulse chemisorption of the 2%Pd@mTiO₂ indicated that the dispersion of palladium in 2%Pd@mTiO₂ is 1.51% and the palladium surface area on the amorphous TiO₂ is 6.71m²/g.

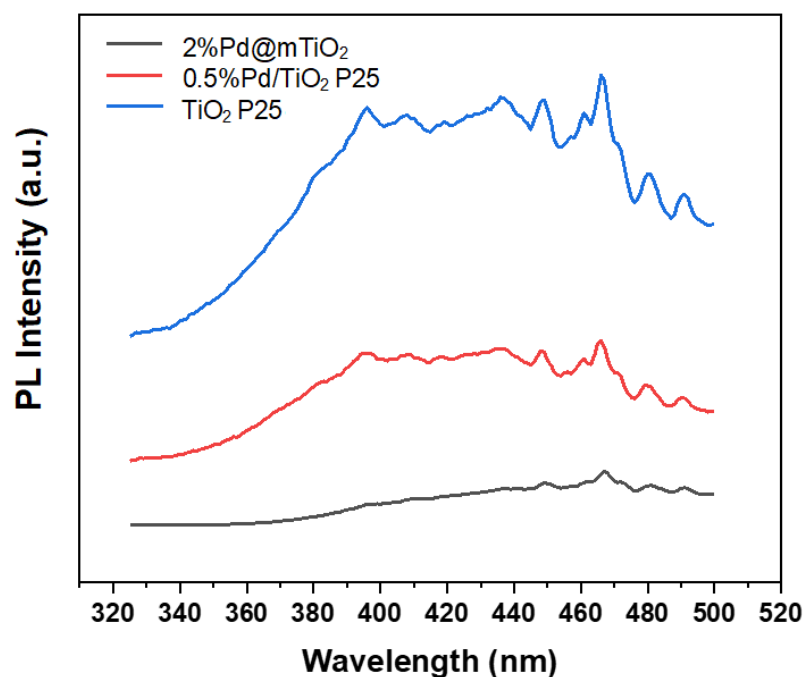


Figure 4. The photoluminescence emission spectra of pristine TiO₂ P25, 0.5%Pd/TiO₂ and 2%Pd@mTiO₂ core@shell nanoparticles.

The thermogravimetric analysis of the pristine TiO₂ P25, 0.5%Pd/TiO₂ P25, and 2%Pd@mTiO₂ core@shell nanoparticles showed distinctive curves which correspond to the weight loss in the catalyst. In the first step, the weight loss is between 10 °C and 122 °C, which corresponds to the removal of volatile organic solvents like n-hexane, methanol and 1-butanol used in the preparation of the core@shell nanoparticles. The second weight loss is between 122 °C and 250 °C, which is due to physisorbed water on the photocatalyst, and the third weight loss occurs between 250 °C and 355 °C, which could be assigned to the high-temperature pyrolysis of carbon species from the CTAB used in catalyst preparation. The fourth step is above 444 °C, which could be assigned to loss accompanied by the collapse of the core@shell moieties.

The Pd metal content of both fresh and spent 0.5%Pd/TiO₂ P25 and 2%Pd@mTiO₂ core@shell nanoparticles was evaluated using ICP-OES analysis (Table 1). The 2%Pd@mTiO₂ nanoparticles showed 1.8% palladium in the fresh catalyst, and 1.78% palladium in the spent 2%Pd@mTiO₂ catalyst, which was recovered after four cycles in the reusability studies. In comparison, the 0.5%Pd/TiO₂ P25 catalyst showed 0.43% palladium in the fresh catalyst, and 0.33% palladium in the spent catalyst recovered after the fourth cycle. The Pd metal content indicated the higher stability of 2%Pd@mTiO₂ core@shell nanoparticles than conventional 0.5%Pd/TiO₂ P25 catalysts.

Table 1. The ICP-OES results for the catalyst.

| Catalysts | ICP Analysis (%) | |
|-------------------------|------------------|------------|
| | Fresh (%Pd) | Used (%Pd) |
| 0.5%Pd-TiO ₂ | 0.43 | 0.33 |
| 2%Pd@TiO ₂ | 1.8 | 1.78 |

3.2. Photocatalytic Degradation of Phenol Using Batch Photoreactor

The photocatalytic degradation of phenol was performed in a batch photoreactor with TiO₂ P25, 0.5%Pd/TiO₂ P25 and 2%Pd@mTiO₂ catalysts with oxygen, using UV and visible light. The corresponding plots of the total concentration of phenol as a function

of time are shown in Figure 5. From the comparison of TiO₂ P25, 0.5%Pd/TiO₂ P25 and 2%Pd@mTiO₂ photocatalysts, in the presence of UV light (Figure 5a), the 0.5%Pd/TiO₂ P25 catalyst showed the maximum phenol degradation rate, with 79.7% phenol conversion to CO₂ and H₂O after 120 min with O₂, whereas the TiO₂ P25 catalyst showed 64.6% phenol conversion, and the 2%Pd@mTiO₂ catalyst achieved 53.7% conversion of phenol. The improved photocatalytic activity of 0.5%Pd/TiO₂ P25 catalyst, in UV light could be attributed to presence of surface Pd nanoparticles, acting as a trap centre for the electrons generated, and thus reducing the recombination rate of the charge carriers. In contrast, when photocatalytic degradation of phenol was studied under identical reaction conditions, using visible light instead of UV light, the 2%Pd@mTiO₂ catalyst showed the highest photodegradation activity, resulting in 50% phenol conversion, while 0.5%Pd/TiO₂ P25 and TiO₂ P25 showed only 25.1% and 18.3% phenol conversion, respectively. In visible light irradiation, the improved photodegradation activity of the 2%Pd@mTiO₂ catalyst could be attributed to a combination of factors such as the increased absorbance in the visible region, the higher specific surface area, and the reduced electron–hole pair recombination rate.

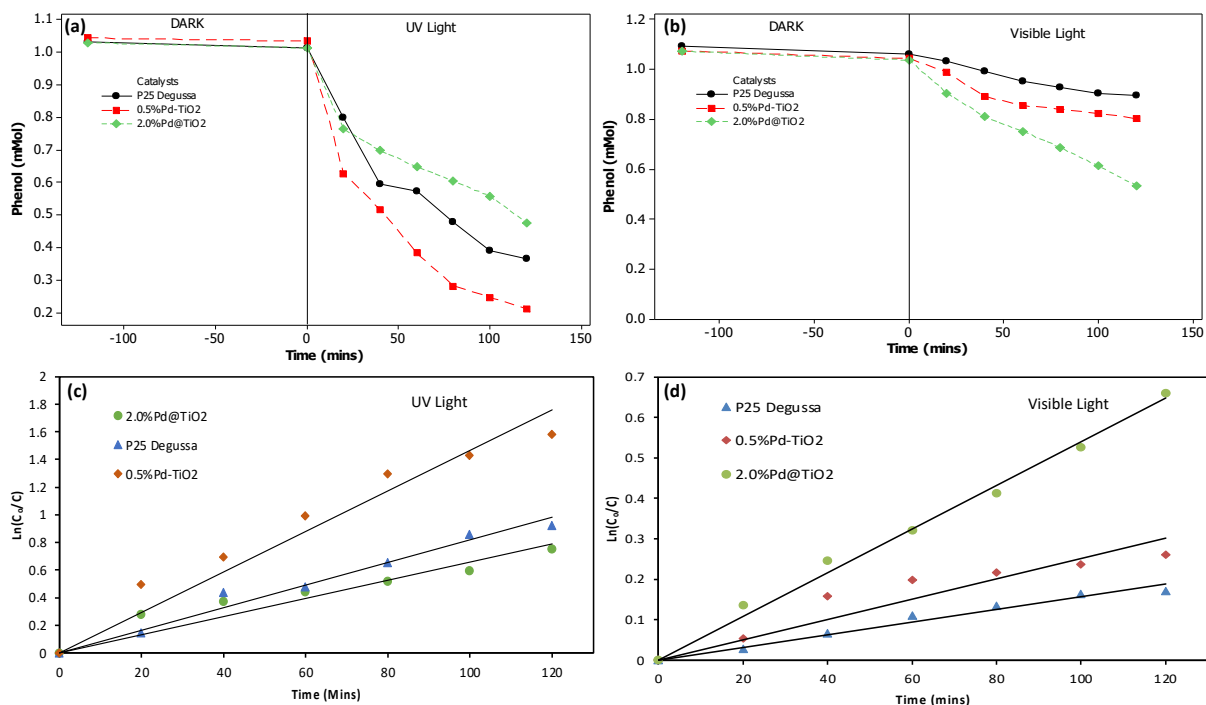


Figure 5. (a) Photocatalytic degradation of phenol with TiO₂ P25, 0.5%Pd-TiO₂ and 2%Pd@mTiO₂ catalysts in batch reactor using UV light, with oxygen as the oxidant. (b) Photocatalytic degradation of phenol in batch reactor using visible light, with oxygen as the oxidant. (c) Pseudo-first-order kinetics of photocatalytic degradation of phenol in UV light. (d) Pseudo-first-order kinetics of photocatalytic degradation of phenol in visible light.

The photocatalytic degradation of organic pollutants is often determined by using pseudo-first-order kinetics [47–49]. The initial rate of phenol degradation was determined after the first 20 min of the reaction, assuming pseudo-first-order kinetics with respect to the phenol concentration.

$$r = \frac{dC}{dt} = k_{obs}C \quad (1)$$

Integrating Equation (1) above with the restriction $C = C_0$ at $t = 0$, with C_0 being the initial phenol concentration and t , the reaction time yields the following expression:

$$\ln\left(\frac{C_0}{C}\right) = k_{obs}t \quad (2)$$

The expression k_{obs} in the above equation is the apparent pseudo-first-order rate constant and depends on the phenol concentration. The plot of $\ln(C_0/C)$ as a function of time for phenol degradation, using the batch photoreactor in O_2 with the different photocatalysts in UV and visible light, is shown in Figure 5c,d. The corresponding photodegradation rate constants for phenol and the quantum efficiencies obtained with each photocatalyst are summarized in Table 2.

Table 2. The rate of the photocatalytic mineralization of phenol with the quantum efficiencies.

| Catalysts | UV Light | | | Visible Light | |
|-------------------------|---|-------------------------|-----------------------|---|-------------------------|
| | Rate Constant k_{abs} (10^{-4} s^{-1}) | Phenol Converted (%) | Quantum Efficiency | Rate Constant k_{abs} (10^{-4} s^{-1}) | Phenol Converted (%) |
| TiO ₂ P25 | 1.37 | 64.6 | 0.73 | 0.27 | 18.3 |
| 0.5%Pd/TiO ₂ | 2.45 | 79.7 | 0.94 | 0.42 | 25.1 |
| 2%Pd@mTiO ₂ | 1.1 | 53.7 | 0.61 | 0.9 | 50.0 |

Further analysis of the reaction mixture indicated that the formation of intermediates like catechol, pyrogallol and benzoquinone, and the polymerization of phenol occurred immediately after the first 20 min of irradiation with UV light. This was suggested from the brownish colour that formed, which slowly disappeared upon further conversion of intermediates to CO_2 and water. It is suggested that the polymer was subsequently transformed to hydroxylated products, like the intermediates formed in the degradation of phenol, which further oxidized to CO_2 and water.

3.3. Photocatalytic Degradation of Phenol Using Continuous Flow Trickle Bed and Taylor Flow Photoreactors

Taking into consideration the effect of mass transfer limitation, the phenol photodegradation process was redesigned to operate continuously with an increase in the dissolution of the oxygen used as an oxidant; the trickle-bed and Taylor flow photoreactors were used with the 2%Pd@mTiO₂ catalyst, using UV light. UV light irradiation was chosen over visible light to study the effect of reactor configuration, to ensure decent photodegradation activity from TiO₂ P25, to further evaluate how much we can improve the photodegradation performance owing to improved mass transfer by using the Taylor flow in comparison to the traditional trickle-bed. The trickle-bed is a packed-bed reactor, while the Taylor flow showed a distinct separation of gas liquid slugs in flow, where oxygen replenished the catalyst surface continually. Using the trickle-bed photoreactor with UV light, 85% phenol conversion to CO_2 and water was achieved, while in the Taylor flow system, 97% photodegradation of phenol was achieved (Figure 6). In comparison, the batch photoreactor showed only 53.7% conversion of phenol (Figure 5a). The significant improvement in the phenol photodegradation in the continuous flow photoreactors was due to the increase in the availability of the oxygen needed for the photodegradation reaction. In the Taylor flow system, alternating the slug of the phenol solution (liquid) with the oxygen gas bubble increased the rate of the reaction. In the literature, the photocatalytic degradation of phenol has been extensively investigated, and its degradation proceeds predominately via $\cdot OH$ radicals [50,51]. Thus, it is suggested that the Taylor flow system could enhance the reaction rate by increasing the production of $\cdot OH$ radicals in the presence of oxygen on the surface of the 2%Pd@mTiO₂ catalyst. It is also well established that the photocatalytic activity is enhanced by the effective separation and transportation of photogenerated charge carriers. For the 2%Pd@mTiO₂ catalyst, with the decrease in the recombination of electron–hole pairs, more electrons and holes will be involved in the photocatalytic degradation of phenol. We proposed the photocatalytic mechanism of 2%Pd@mTiO₂ catalyst, as shown in Scheme 2. As seen in Figure 2b, the UV-Vis spectra of the 2%Pd@mTiO₂ catalyst shows strong absorption in the visible region, while the pristine TiO₂ P25 and 0.5%Pd/TiO₂ P25 catalysts do not absorb in the visible light region of the spectrum. The presence of Pd nanoparticles

contributes to the formation of electron–hole pairs under visible light illumination via a combination of three different ways: by extending the light absorption of TiO₂ to longer wavelengths; increasing the scattering of visible light; and creating electron–hole pairs by transferring the electrons from the Pd nanoparticles to the conduction band of TiO₂.

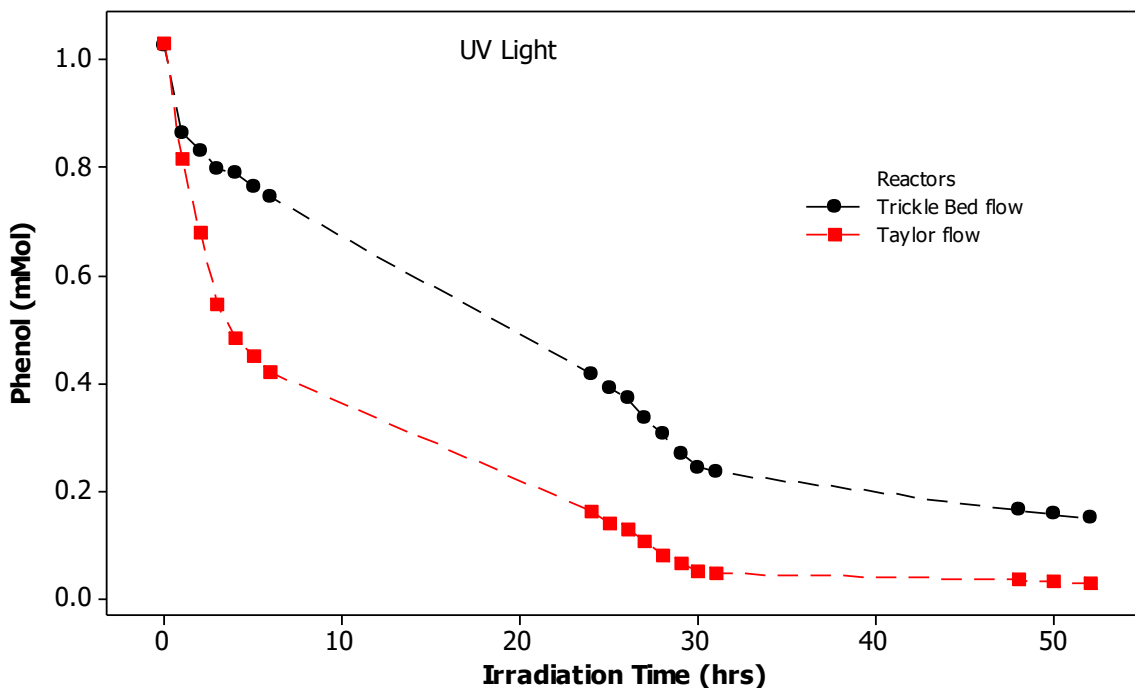
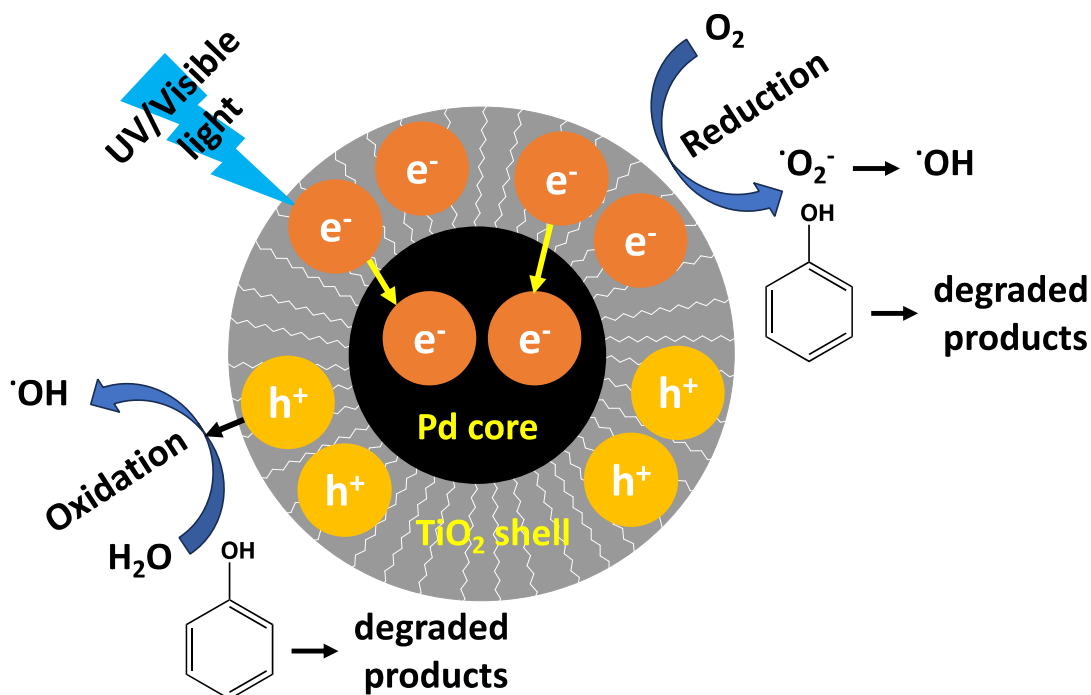


Figure 6. Photocatalytic degradation of phenol with 2%Pd@mTiO₂ catalyst in oxygen, using continuous flow trickle-bed and Taylor flow reactors.



Scheme 2. Proposed mechanism for photocatalytic degradation of phenol with 2%Pd@mTiO₂.

3.4. Effect of Photolysis

In control experiments, the photolysis of phenol was investigated in UV light without catalyst using the batch photoreactor to examine the effect of UV light and oxidant on phenol photodegradation. As shown in Figure 7, the degradation of phenol using UV light in 120 min was 42.2%, 32.2%, 28.5% and 8.8% with 1.39M of H₂O₂, 0.174M of H₂O₂, oxygen gas and nitrogen, respectively. There was no significant degradation of the phenol with the UV light in nitrogen atmosphere. These results indicate that the degradation of phenol was mainly caused by photolysis in the absence of the catalyst; however, the presence of the oxidizing species was essential for the complete photodegradation of phenol in photocatalysis.

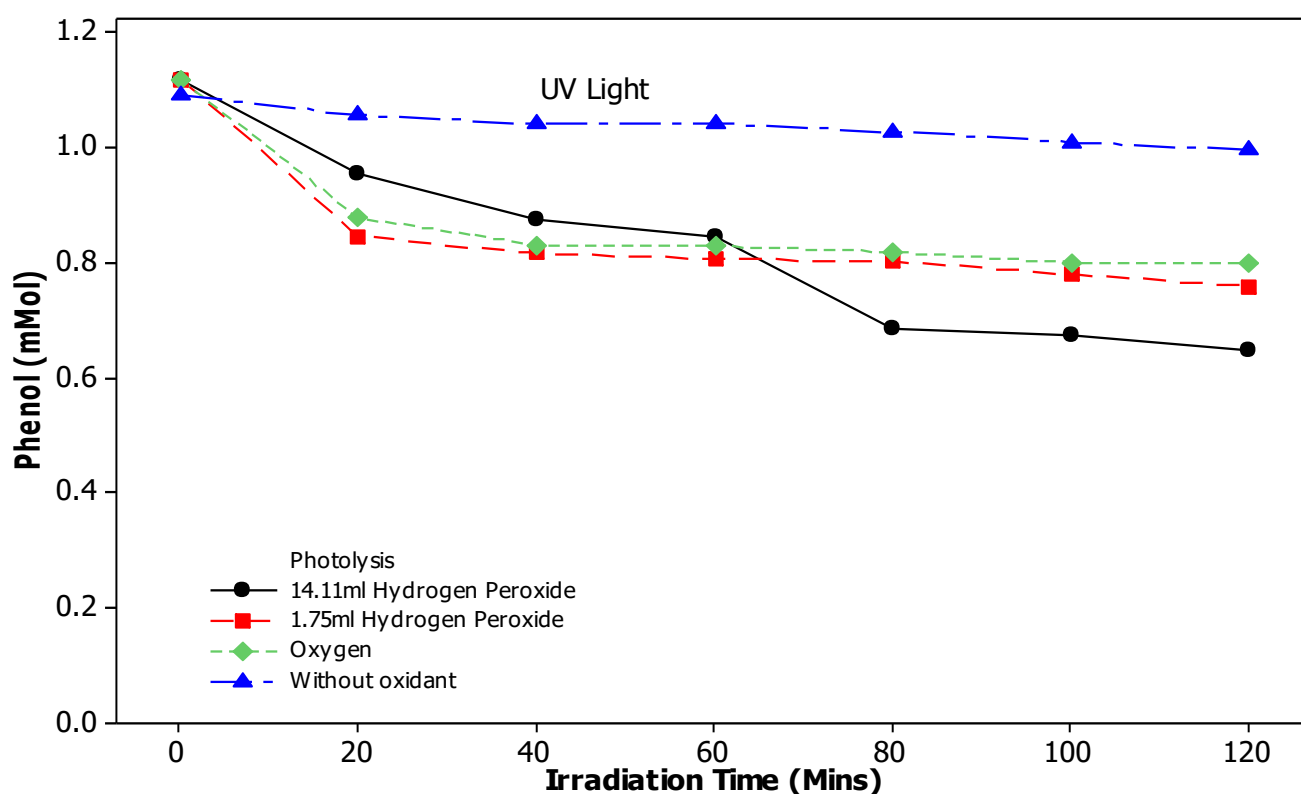


Figure 7. Phenol photolysis with UV light using hydrogen peroxide and oxygen.

3.5. Reusability of Catalyst

To develop a continuous process, the stability and reusability of any photocatalyst are critical for potential practical applications. The stability and reusability of the photocatalysts were evaluated using 0.2 g of the photocatalyst in 94.11 mg/L of phenol solution. Post reaction, TiO₂ P25, 0.5%Pd/TiO₂ P25 and 2%Pd@mTiO₂ catalysts were recovered by filtration, washed, dried, and evaluated for reusability under the same experimental conditions, over four recycles (Figure 8). Significant loss in activity was observed for the 0.5%Pd/TiO₂ P25 and TiO₂ P25 catalysts, which could be due to metal leaching as well as the poisoning of the catalyst surface due to the deposition of polymeric species or reaction intermediates, indicated from the colour change of the spent catalyst to black. The Pd metal content of the fresh and used 0.5%Pd/TiO₂ P25 catalyst using ICP-OES analysis (Table 1) showed a noticeable decrease in Pd content on the used catalyst, due to metal leaching. Using the 2%Pd@mTiO₂ catalyst, noticeable stable photodegradation activity was achieved, with phenol % conversion only marginally decreasing from 53.7% to 50.4% in the fourth reuse. The 2%Pd@mTiO₂ catalyst also exhibited stability towards metal leaching and photocorrosion, as indicated by the palladium metal content (Table 1).

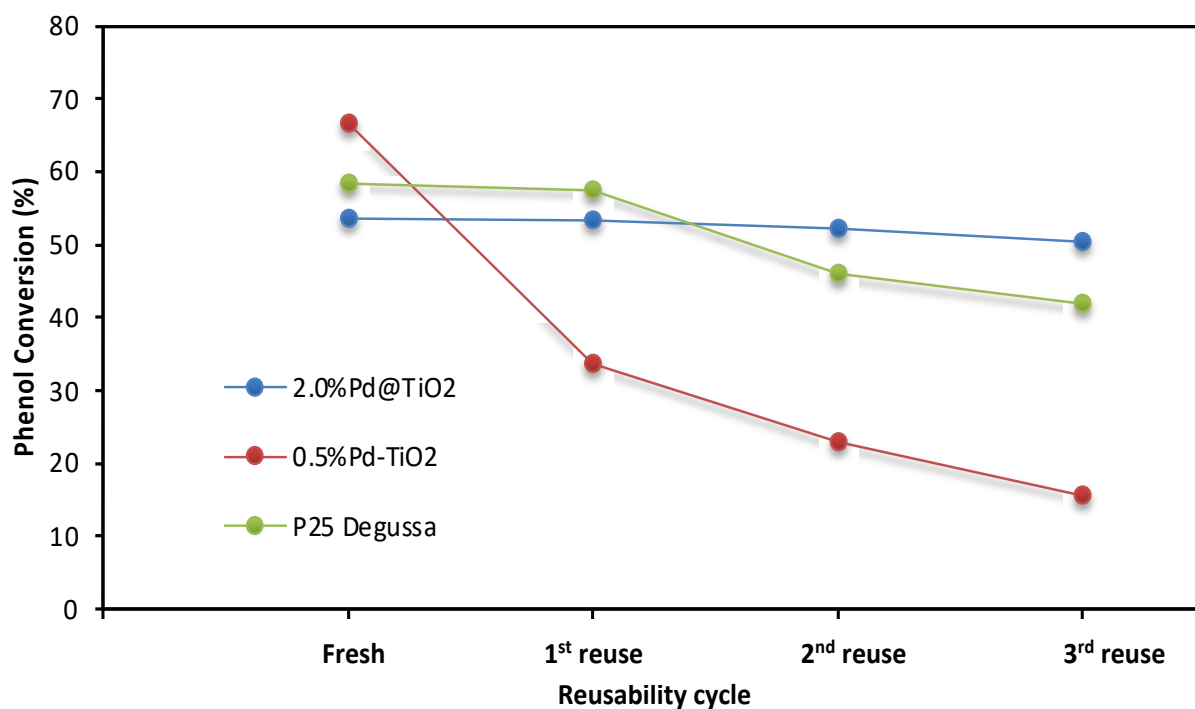


Figure 8. Reusability of 2%Pd@mTiO₂ in photodegradation of phenol in oxygen in the batch photoreactor.

Although 2.0%Pd@mTiO₂ catalyst was less active in UV light than the 0.5%Pd/TiO₂ P25 catalyst, but much more active in visible light, its stability towards leaching is a significant advantage over 0.5%Pd/TiO₂ P25.

To further confirm the deposition of intermediates on the used catalyst, temperature-programmed oxidation studies were performed for the used catalyst. The deposited intermediates on the catalyst surface were observed to desorb at 310 °C.

4. Conclusions

In this study, 2%Pd@mTiO₂ core@shell nanoparticles with a uniform and narrow particle size distribution were successfully synthesised using a four-component “water in oil” microemulsion system. The prepared 2%Pd@mTiO₂ core@shell nanoparticles showed very good absorption in both the UV and visible regions, and a low bandgap of 1.67 eV, indicating high suitability as visible light photocatalysts. The prepared 2%Pd@mTiO₂ core@shell nanoparticles showed better photocatalytic performance for phenol degradation in visible light in comparison to pristine TiO₂ P25 and conventional 0.5%Pd/TiO₂ P25 catalysts, in batch and continuous flow trickle-bed and Taylor flow photoreactors. The 0.5%Pd/TiO₂ P25 catalyst showed higher phenol photodegradation activity in UV light, while the 2%Pd@mTiO₂ catalyst showed superior photocatalytic activity under visible light illumination in terms of phenol degradation to CO₂ and water. The 2%Pd@mTiO₂ catalyst also showed excellent stability and reusability in comparison to the TiO₂ P25 and 0.5%Pd/TiO₂ P25 catalysts. The photodegradation of phenolics is limited by mass transfer with respect to the availability of oxygen on the catalyst surface. The performance of the prepared catalyst in terms of phenol photodegradation was enhanced by using a continuous Taylor flow system, with 97% of 300 mL phenol solution passed into the continuous reactor at a flow rate of 0.083 mL/min being degraded in 52 h. The 2%Pd@mTiO₂ core@shell nanoparticles performed with superior photodegradation activity in visible light with improved stability as photocatalysts as compared to TiO₂ P25 and 0.5%Pd/TiO₂ P25.

Supplementary Materials: The following supporting information can be downloaded at <https://www.mdpi.com/article/10.3390/w15162975/s1>, Figure S1. An example of HPLC chromatogram.

Author Contributions: Conceptualisation, H.M.; methodology, H.M., D.R. and M.T.Y.; validation, M.T.Y. and H.M.; resources, H.M., D.R. and N.A.; writing—original draft preparation, M.T.Y.; writing—review and editing, H.M., N.A. and D.R.; supervision, H.M. and D.R.; project administration, H.M. and D.R.; funding acquisition, H.M. and D.R. All authors have read and agreed to the published version of the manuscript.

Funding: This research received no external funding.

Data Availability Statement: Not applicable.

Acknowledgments: The authors gratefully acknowledge financial support from Queens University Belfast and the STEP-B of National Research Institute for Chemical Technology (NARICT), Zaria, as well as the recent collaboration between the School of Chemistry and Chemical Engineering at QUB and NARICT.

Conflicts of Interest: The authors declare no conflict of interest. The funders had no role in the design of the study; in the collection, analyses, or interpretation of data; in the writing of the manuscript; or in the decision to publish the results.

References

1. Beltran, F.J.; Rivas, F.J.; Gimeno, O. Comparison between photocatalytic ozonation and other oxidation processes for the removal of phenols from water. *J. Chem. Technol. Biotechnol.* **2005**, *80*, 973–984. [[CrossRef](#)]
2. Adan, C.; Coronado, J.M.; Bellod, R.; Soria, J.; Yamaoka, H. Photochemical and photocatalytic degradation of salicylic acid with hydrogen peroxide over TiO₂/SiO₂ fibres. *Appl. Catal. A Gen.* **2006**, *303*, 199–206. [[CrossRef](#)]
3. Su, R.; Tiruvalam, R.; He, Q.; Dimitratos, N.; Kesavan, L.; Hammond, C.; Lopez-Sanchez, J.A.; Bechstein, R.; Kiely, C.J.; Hutchings, G.J.; et al. Promotion of phenol photodecomposition over TiO₂ using Au, Pd and Au-Pd Nanoparticles. *ACS Nano* **2012**, *6*, 6284–6292. [[CrossRef](#)] [[PubMed](#)]
4. Dionysiou, D.D.; Khodadoust, A.P.; Kern, A.M.; Suidan, M.T.; Baudin, I.; Laine, J.-M. Continuous-mode photocatalytic degradation of chlorinated phenols and pesticides in water using a bench-scale TiO₂ rotating disk reactor. *Appl. Catal. B Environ.* **2000**, *24*, 139–155. [[CrossRef](#)]
5. Pérez, M.H.; Peñuela, G.; Maldonado, M.I.; Malato, O.; Pilar, F.-I.; Oller, I.; Gernjak, W.; Malato, S. Degradation of pesticides in water using solar advanced oxidation processes. *Appl. Catal. B Environ.* **2006**, *64*, 272–281. [[CrossRef](#)]
6. Ghumro, S.S.; Lal, B.; Pirzada, T. Visible-Light-Driven Carbon-Doped TiO₂-Based Nanocatalysts for Enhanced Activity toward Microbes and Removal of Dye. *ACS Omega* **2022**, *7*, 4333–4341. [[CrossRef](#)]
7. Park, B.G. Photocatalytic activity of TiO₂-doped Fe, Ag, and Ni with N under visible light irradiation. *Gels* **2022**, *8*, 14. [[CrossRef](#)]
8. Sirivallop, A.; Areerob, T.; Chiarakorn, S. Enhanced Visible Light Photocatalytic Activity of N and Ag Doped and Co-Doped TiO₂ Synthesized by Using an In-Situ Solvothermal Method for Gas Phase Ammonia Removal. *Catalysts* **2020**, *10*, 251. [[CrossRef](#)]
9. Al-Hamoud, K.; Shaik, M.R.; Khan, M.; Alkhatlan, H.Z.; Adil, S.F.; Kuniyil, M.; Assal, M.E.; Al-Warthan, A.; Siddiqui, M.R.H.; Tahir, M.N.; et al. *Pulicaria undulata* Extract-Mediated Eco-Friendly Preparation of TiO₂ Nanoparticles for Photocatalytic Degradation of Methylene Blue and Methyl Orange. *ACS Omega* **2022**, *7*, 4812–4820. [[CrossRef](#)]
10. Shubha, J.P.; Adil, S.F.; Khan, M.; Hatshan, M.R.; Khan, A. Facile Fabrication of a ZnO/Eu₂O₃/NiO-Based Ternary Heterostructure Nanophotocatalyst and Its Application for the Degradation of Methylene Blue. *ACS Omega* **2021**, *5*, 3866–3874. [[CrossRef](#)]
11. Gerven, T.V.; Stankiewicz, A. Structure, energy, synergy, time—The fundamentals of process intensification. *Ind. Eng. Chem. Res.* **2009**, *48*, 2465–2474. [[CrossRef](#)]
12. Cassano, A.E.; Martin, C.A.; Brandi, R.J.; Alfano, O.M. Photoreactor analysis and design: Fundamentals and applications. *Ind. Eng. Chem. Res.* **1995**, *34*, 2155–2201. [[CrossRef](#)]
13. Yue, P.L. Modelling, scale-up and design of multiphasic photoreactors. In *Photocatalytic Purification and Treatment of Water and Air*; Ollis, D.F., Al-Ekabi, H., Eds.; Elsevier Science Publishers BV: Amsterdam, The Netherlands, 1993; pp. 495–510.
14. Sclafani, A.; Brucato, A.; Rizzuti, L. Mass transfer limitations in a packed bed photoreactor used for phenol removal. In *Photocatalytic Purification and Treatment of Water and Air*; Ollis, D.F., Al-Ekabi, H., Eds.; Elsevier Science Publishers BV: Amsterdam, The Netherlands, 1993; pp. 533–545.
15. Szechowski, J.G.; Koval, C.A.; Noble, R.D. A Taylor vortex reactor for heterogeneous photocatalysis. *Chem. Eng. Sci.* **1995**, *50*, 3163–3173. [[CrossRef](#)]
16. Haarstrick, A.; Kut, O.M.; Heinze, E. TiO₂ assisted degradation of environmentally relevant organic compounds in wastewater using a novel fluidized bed photoreactor. *Environ. Sci. Technol.* **1996**, *30*, 817–824. [[CrossRef](#)]
17. Ollis, D.F.; Pelizzetti, E.; Serpone, N. *Photocatalysis: Fundamentals and Applications*; Wiley: New York, NY, USA, 1989.
18. Peill, N.J.; Hoffmann, M.R. Development and optimization of a TiO₂-coated fiber-optic cable reactor: Photocatalytic degradation of 4-chlorophenol. *Environ. Sci. Technol.* **1995**, *29*, 2974–2981. [[CrossRef](#)]

19. Ray, A.K.; Beenackers, A.A.C.M. Novel swirl flow reactor for kinetic studies of semiconductor photocatalysis. *AIChE J.* **1997**, *43*, 2571–2578. [[CrossRef](#)]
20. Amoli-Diva, M.; Anvari, A.; Sadighi-Bonabi, R. Synthesis of magneto-plasmonic Au-Ag NPs-decorated TiO₂-modified Fe₃O₄ nanocomposite with enhanced laser/solar-driven photocatalytic activity for degradation of dye pollutant in textile wastewater. *Ceram. Int.* **2019**, *45*, 17837–17846. [[CrossRef](#)]
21. Mondal, K.; Sharma, A. Recent advances in the synthesis and application of photocatalytic metal-metal oxide core-shell nanoparticles for environmental remediation and their recycling process. *RSC Adv.* **2016**, *6*, 83589–83612. [[CrossRef](#)]
22. Lu, F.F.; Dong, A.Q.; Ding, G.J.; Xu, K.; Li, J.M.; You, L.J. Magnetic porous polymer composite for high performance adsorption of acid red 18 based on melamine resin and chitosan. *J. Mol. Liq.* **2019**, *294*, 111515. [[CrossRef](#)]
23. Du, D.; Shi, W.; Wang, L.Z.; Zhang, J.L. Yolk-shell structured Fe₃O₄@void@TiO₂ as a photo-Fenton-like catalyst for the extremely efficient elimination of tetracycline. *Appl. Catal. B* **2017**, *200*, 484–492. [[CrossRef](#)]
24. Min, Y.; Song, G.; Zhou, L.; Wang, X.; Liu, P.; Li, J. Silver@mesoporous Anatase TiO₂ Core-Shell Nanoparticles and Their Application in Photocatalysis and SERS Sensing. *Coatings* **2022**, *12*, 64. [[CrossRef](#)]
25. Bayles, A.; Tian, S.; Zhou, J.; Yuan, L.; Yuan, Y.; Jacobson, C.R.; Farr, C.; Zhang, M.; Swearer, D.F.; Solti, D.; et al. Al@TiO₂ Core-Shell Nanoparticles for Plasmonic Photocatalysis. *ACS Nano* **2022**, *16*, 5839–5850. [[CrossRef](#)] [[PubMed](#)]
26. Deshmukh, G.; Manyar, H. *Advanced Oxidation Processes for Wastewater Treatment, Advanced Materials and Technologies for Wastewater Treatment*; CRC Press: Boca Raton, FL, USA, 2021; pp. 153–164.
27. Morrison, G.; Bannon, R.; Wharry, S.; Moody, T.S.; Mase, N.; Hattori, M.; Manyar, H.; Smyth, M. Continuous flow photooxidation of alkyl benzenes using fine bubbles for mass transfer enhancement. *Tetrahed. Lett.* **2022**, *90*, 153613. [[CrossRef](#)]
28. Yadav, G.D.; Mewada, R.K.; Wagh, D.W.; Manyar, H. Advances and future trends in selective oxidation catalysis: A critical review. *Catal. Sci. Technol.* **2022**, *12*, 7245. [[CrossRef](#)]
29. Ethiraj, J.; Wagh, D.; Manyar, H. Advances in upgrading biomass to biofuels and oxygenated fuel additives using metal oxide catalysts. *Energy Fuels* **2022**, *36*, 1189–1204. [[CrossRef](#)]
30. Skillen, N.; Ralphs, K.; Craig, D.; McCalmont, S.; Muzio, A.F.V.; O'Rourke, C.; Manyar, H.; Robertson, P.K.J. Photocatalytic reforming of glycerol to H₂ in a thin film Pt-TiO₂ recirculating photoreactor. *J. Chem. Technol. Biotech.* **2020**, *95*, 2619–2627.
31. Yilleng, M.T.; Gimba, E.C.; Ndukwe, G.I.; Bugaje, I.M.; Rooney, D.W.; Manyar, H.G. Batch to continuous photocatalytic degradation of phenol using TiO₂ and Au-Pd nanoparticles supported on TiO₂. *J. Environ. Chem. Eng.* **2018**, *6*, 6382–6389. [[CrossRef](#)]
32. Yadav, G.D.; Manyar, H.G. Synthesis of a novel redox material UDcaT-3: An efficient and versatile catalyst for selective oxidation, hydroxylation and hydrogenation reactions. *Adv. Syn. Catal.* **2008**, *350*, 2286–2294. [[CrossRef](#)]
33. Manyar, H.G.; Chaure, G.S.; Kumar, A. The green catalytic oxidation of alcohols in water by using highly efficient manganosilicate molecular sieves. *Green Chem.* **2006**, *8*, 344–348. [[CrossRef](#)]
34. Jakubek, T.; Hudy, C.; Gryboś, J.; Manyar, H.; Kotarba, A. Thermal transformation of birnessite (OL) towards highly active cryptomelane (OMS-2) catalyst for soot oxidation. *Catal. Lett.* **2019**, *149*, 2218–2225. [[CrossRef](#)]
35. Jakubek, T.; Ralphs, K.; Kotarba, A.; Manyar, H. Nanostructured potassium-manganese oxides decorated with Pd nanoparticles as efficient catalysts for low-temperature soot oxidation. *Catal. Lett.* **2019**, *149*, 100–106. [[CrossRef](#)]
36. McManus, I.J.; Daly, H.; Manyar, H.G.; Taylor, S.F.R.; Thompson, J.M.; Hardacre, C. Selective hydrogenation of halogenated arenes using porous manganese oxide (OMS-2) and platinum supported OMS-2 catalysts. *Faraday Discuss.* **2016**, *188*, 451–466. [[CrossRef](#)] [[PubMed](#)]
37. O'Donnell, R.; Ralphs, K.; Grolleau, M.; Manyar, H.; Artioli, N. Doping Manganese Oxides with Ceria and Ceria Zirconia Using a One-Pot Sol-Gel Method for Low Temperature Diesel Oxidation Catalysts. *Top. Catal.* **2020**, *63*, 351–362. [[CrossRef](#)]
38. Coney, C.; Hardacre, C.; Morgan, K.; Artioli, N.; York, A.P.E.; Millington, P.; Kolpin, A.; Goguet, A. Investigation of the oxygen storage capacity behaviour of three way catalysts using spatio-temporal analysis. *Appl. Catal. B Environ.* **2019**, *258*, 117918. [[CrossRef](#)]
39. Castoldi, L.; Matarrese, R.; Kubiak, L.; Daturi, M.; Artioli, N.; Pompa, S.; Lietti, L. In-depth insights into N₂O formation over Rh- and Pt-based LNT catalysts. *Catal. Today* **2019**, *320*, 141–151. [[CrossRef](#)]
40. Salisu, J.; Gao, N.; Quan, C.; Yanik, J.; Artioli, N. Co-gasification of rice husk and plastic in the presence of CaO using a novel ANN model-incorporated Aspen plus simulation. *J. Energy Inst.* **2023**, *108*, 101239. [[CrossRef](#)]
41. Quan, C.; Zhang, G.; Gao, N.; Su, S.; Artioli, N.; Feng, D. Behavior Study of Migration and Transformation of Heavy Metals during Oily Sludge Pyrolysis. *Energy Fuels* **2022**, *36*, 8311–8322. [[CrossRef](#)]
42. Byrne, E.L.; O'Donnell, R.; Gilmore, M.; Artioli, N.; Holbrey, J.D.; Swadzba-Kwasny, M. Hydrophobic functional liquids based on trioctylphosphine oxide (TOPO) and carboxylic acids. *Phys. Chem. Chem. Phys.* **2020**, *22*, 24744–24763. [[CrossRef](#)]
43. Pandit, K.; Jeffrey, C.; Keogh, J.; Tiwari, M.S.; Artioli, N.; Manyar, H.G. Techno-Economic Assessment and Sensitivity Analysis of Glycerol Valorization to Biofuel Additives via Esterification. *Ind. Eng. Chem. Res.* **2023**, *62*, 9201–9210. [[CrossRef](#)]
44. Manyar, H.G.; Iliade, P.; Bertinetti, L.; Coluccia, S.; Berlier, G. Structural and spectroscopic investigation of ZnS nanoparticles grown in quaternary reverse micelles. *J. Coll. Interface Sci.* **2011**, *354*, 511–516. [[CrossRef](#)]
45. Yaemsunthorn, K.; Kobielski, M.; Macyk, W. TiO₂ with Tunable Anatase-to-Rutile Nanoparticles Ratios: How Does the Photoactivity Depend on the Phase Composition and the Nature of Photocatalytic Reaction. *ACS Appl. Nano Mater.* **2021**, *4*, 633–643. [[CrossRef](#)]

46. Ohde, H.; Wai, C.M.; Kim, H.; Kim, J.; Ohde, M. Hydrogenation of olefins in supercritical CO₂ catalyzed by palladium nanoparticles in a water-in-CO₂ microemulsion. *J. Am. Chem. Soc.* **2002**, *124*, 4540–4541. [[CrossRef](#)] [[PubMed](#)]
47. Xu, P.; Zeng, G.; Huang, D.; Liu, L.; Lai, C.; Chen, M.; Zhang, C.; He, X.; Lai, M.; He, Y. Photocatalytic degradation of phenol by the heterogeneous Fe₃O₄ nanoparticles and oxalate complex system. *RSC Adv.* **2014**, *4*, 40828–40836. [[CrossRef](#)]
48. Hamza, A.; Fatuase, J.T.; Waziri, S.M.; Ajayi, O.A. Solar Photocatalytic degradation of phenol using nanosized ZnO and α-Fe₂O₃. *J. Chem. Eng. and Mat. Sci.* **2013**, *4*, 87–92.
49. Qiu, R.; Song, L.; Mo, Y.; Zhang, D.; Brewer, E. Visible light induced photocatalytic degradation of phenol by polymer- modified semiconductors: Study of the influencing factors and the kinetics. *Reac. Kinet. Catal. Lett.* **2008**, *94*, 183–189. [[CrossRef](#)]
50. Ilisz, A.; La, Z. Investigation of the photodecomposition of phenol in near UV irradiated aqueous TiO₂ suspensions. I: Effect of charge-trapping species on the degradation kinetics. *Appl. Catal. A Gen.* **1999**, *180*, 25–33. [[CrossRef](#)]
51. Park, H.; Choi, W. Photocatalytic conversion of benzene to phenol using modified TiO₂ and polyoxometalates. *Catal. Today* **2005**, *101*, 291–297. [[CrossRef](#)]

Disclaimer/Publisher's Note: The statements, opinions and data contained in all publications are solely those of the individual author(s) and contributor(s) and not of MDPI and/or the editor(s). MDPI and/or the editor(s) disclaim responsibility for any injury to people or property resulting from any ideas, methods, instructions or products referred to in the content.